Lasers in Surgery and Medicine 18:410–419 (1996)

Dynamic T1-Weighted Magnetic Resonance Imaging of Interstitial Laser Photocoagulation in the Liver: Observations on In Vivo Temperature Sensitivity

Marvin P. Fried, MD, Paul R. Morrison, MSc, Stephen G. Hushek, PhD, Gilberto A. Kernahan, BSc, and Ferenc A. Jolesz, MD

Department of Otology and Laryngology, Harvard Medical School and Harvard Medical Laser Center, Joint Center for Otolaryngology of Beth Israel and Brigham and Women's Hospitals, Boston, Massachusetts 02115 (M.P.F., P.R.M.); Department of Radiology, Harvard Medical School, Boston, Massachusetts 02115 (F.A.J.); Department of Radiology, Brigham and Women's Hospital, Boston, Massachusetts 02115 (F.A.J., S.G.H., G.A.K.)

Background and Objective: **Magnetic resonance imaging's (MRI) potential to monitor interstitial laser photocoagulation (ILP) has been previously demonstrated and is further tested here with improved spatial and temporal resolution.**
Study Design/Materials and Methods: **In vivo experiments employed fiber-delivered 1,064 nm light (3.0 W, 150 sec) in six rabbit livers monitored under T1-weighted FSE MRI as 1 image/10 sec and a 3 mm thick 8 cm FOV. Image signal intensities (SI) were compared with temperatures (T) at 7, 10, and 15 mm from the fiber.**
Results: **Data showed 33°C < T < 60°C. SI did not vary inverse-linearly with T; changes in the tissue altered the MRI signal interfering with the SI changes due to temperature.**
Conclusion: **MRI cannot map SI-derived temperatures over the entire treatment site. The role of MRI's temperature sensitivity must be coordinated with organ- and dose-specific tissue changes.**

Key words: interstitial laser photocoagulation ILTT, magnetic resonance imaging, minimally invasive surgery, Nd:YAG

INTRODUCTION

Interstitial laser photocoagulation (ILP) is a surgical procedure in which an optical fiber is inserted into tissue, and the absorbed laser light heats and destroys tissue about the fiber's tip [1–3]. From a surgical perspective, ILP has the advantage of being "minimally invasive," reducing trauma in accessing the targeted tissue by using either single or multiple implanted fiber(s) rather than a fully dissecting surgical procedure.

Detailed, real-time information of intraoperative tissue changes throughout the affected volume is needed. Such monitoring during laser irradiation would provide feedback to the surgeon for control of the treatment. Thus, the thermal dose delivered would be expedient and complete with minimized adverse effects to adjacent non-targeted tissue. Indeed, a longstanding impediment to the usefulness of ILP is the inability to

Accepted for publication March 9, 1995.

Address reprint requests to Marvin P. Fried, M.D., Harvard Medical School, Joint Center For Otolaryngology, 333 Longwood Avenue, Boston, MA 02115.

Presented at the Annual Meeting of the American Society for Laser Medicine and Surgery held in Toronto, Canada in April, 1994.

directly visualize the damage being done as the laser light is delivered [4].

Magnetic resonance imaging (MRI) noninvasively produces images with excellent soft tissue resolution [5]. The images can be acquired in multiple and arbitrary planes with potential for three-dimensional monitoring. Unlike x-ray images, MRI uses a prescribed sequence of radiofrequency excitations of the tissue while that tissue resides in a strong magnetic field. The magnetic resonance (MR) signal from a given volume of tissue is dependent on a number of tissue characteristics, one of which is temperature [6,7]. Experiments have studied the usefulness of this temperature sensitivity in monitoring ILP and other treatment modalities involving other thermal mechanisms [8–13]. So-called T1-weighted imaging is particularly temperature sensitive [14,15]. Advances in the field of MRI have delivered fast, temperature-sensitive T1-weighted, imaging techniques that acquire images on time scales appropriate for essentially real-time monitoring of ILP [14–16].

Previous experiments have utilized such techniques with ex vivo tissue in water baths to determine measures of the temperature sensitivity, or have imaged ILP on ex vivo tissue specimens or in vitro gel targets [14–16]. Previous in vivo experiments have focused on the feasibility of ILP rather than on a detailed correlation between image, temperature, and tissue effect. The experiments presented in this report were performed in vivo in rabbit liver and used markedly fast image acquisition (1 image/10 sec) to monitor a relatively small volume of tissue (8 cm field of view and 3 mm slice thickness). Measurements of temperature were taken in the MRI image plane, and the plane was able to be located for histology.

The technique exhibits the advances in MRI that offer the possibility of realistic monitoring of ILP, that is, imaging was performed in real time with optimized spatial resolution. However, the interpretation of such images must be formulated by experiment. Here, we emphasize our observations on MRI's temperature sensitivity in vivo.

MATERIALS AND METHODS

Laser and Magnetic Resonance Imaging Unit

The KTP/Nd:YAG laser (Laserscope, San Jose, CA) was calibrated at 1,064 nm to deliver an average of 3.0 W (6 W at a 50% duty cycle: 0.1 sec on/0.1 sec off) through a 600 μm bare delivery fiber. The interstitial laser exposure duration was approximately 2.5 min for each of the six exposures.

Magnetic resonance imaging noninvasively produces images by recording the tissue response to a prescribed sequence of radiofrequency excitations while that tissue resides in a magnetic field gradient. The resulting two-dimensional gray scale image is composed of an array of pixels, the values of which are the MR signal intensity (SI) values at each point. Magnetic resonance imaging was performed on a 1.5 Tesla clinical imaging unit (General Electric Medical Systems, Milwaukee, WI).

Signal intensity has been shown be temperature dependent. This dependence is due to the temperature dependence of the MR-related tissue parameters T1, T2, and water diffusion (T1 and T2 are the spin-lattice and spin-spin relaxation times, respectively). Magnetic resonance imaging sequences can be defined to weight the image in favor of one of these parameters. In these experiments, images were produced using a temperature-sensitive T1-weighted fast-spin-echo (FSE) sequence with an 18 msec effective TE and a 300 msec TR. A 3 inch receive-only surface coil was used with an 8 cm field of view (FOV). The imaging slice thickness was 3 mm. Images had a resolution of 256 × 128 pixels. Each image took 10 sec to acquire, and each acquisition was separated by a 1 sec interval.

Interstitial Laser Photocoagulation Treatment and Dynamic Magnetic Resonance Imaging

Interstitial laser photocoagulation was performed in vivo in six white New Zealand rabbits (4–5 kg), which were anesthetized with intramuscular injections of 33 mg/kg ketamine and 5 mg/kg xylazine. As illustrated in Figure 1, the left medial lobe of the liver was exposed by laparotomy and pulled through the incision to lay extracorporeally during the treatment. This exposed lobe and the area of incision were covered with surgical gauze saturated with normal saline so that the area would not dehydrate. The optical fiber and a linear thermocouple (TC) array [composed of three 0.005 inch diameter copper constantin thermocouples (Omega, Stamford, CT)] were inserted into the liver parallel to each other, separated by ~6.8 mm. A clamp held the fiber and array at a fixed distance. Temperatures were automatically recorded after the acquisition of each MR image.

Magnetic resonance imaging was used to locate the tissue plane that contained both the TC array and the optical delivery fiber (Fig. 2). Repeated imaging of this plane (dynamic imaging) was performed to observe the effects of the treat-

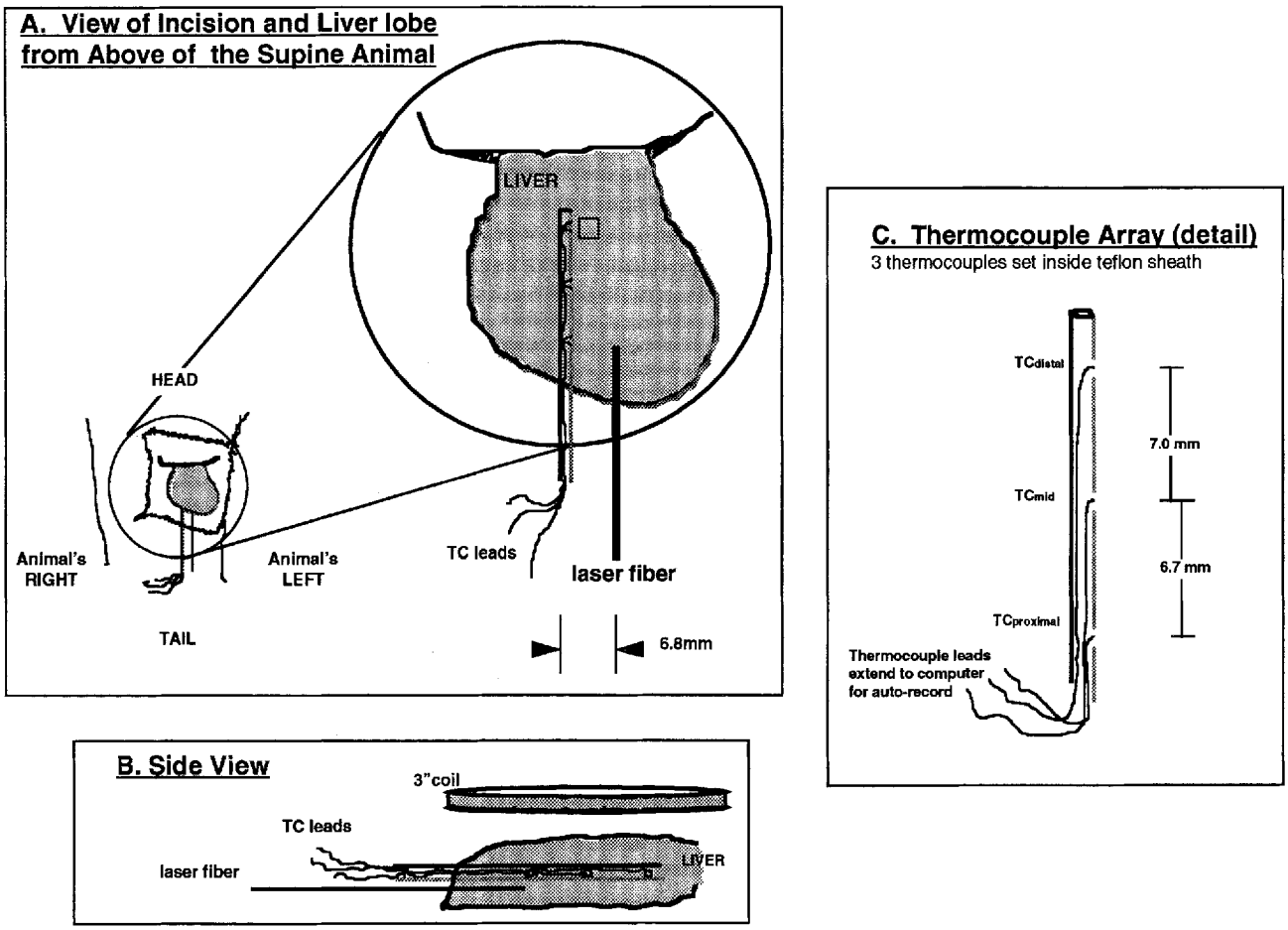

Fig. 1. **A:** On the lower left, a schematic outlines part of the rabbit's torso. An area was shaved and an incision was made just under the ribs. The liver lobe was pulled through. A magnified view shows the placement of the laser fiber alongside the linear array of thermocouples (TCs) at a distance of 6-7 mm. The tip of the laser fiber was set across from the "proximal" thermocouple ($TC_{proximal}$). The small square adjacent to the top TC represents an ROI used in the imaging to determine SI values. **B:** A side view shows the position of the RF receiving coil (not to scale) used in acquiring the MR images. **C:** The thermocouple array was made from a thin-walled Teflon tube with an outer diameter of 2.0 mm. Small windows were cut in the tube wall on one side. Each TC head was glued in place to sit flush with the tube wall. The distances from the fiber tip to each TC were 15.3 mm distal, 9.6 mm mid, and 6.8 mm proximal.

ment. By including the TC array in the imaged plane, image changes were recorded at the sites of temperature measurements (T). Three pretreatment images were acquired, and then approximately 15 images were acquired during the laser exposure. Imaging was continued after the laser exposure for approximately 10 minutes (60–65 images total).

Each MR image was composed of 256 × 128 pixels each with a corresponding value of SI. To obtain measured values of SI at each TC site, average values of SI were calculated by computer from the pixels in a square region of interest (ROI) at each TC in every image (see Fig. 1). With each calculated SI there was an associated standard deviation (sd). The size of the ROI for the first animal was 5 mm^2; a 3 mm^2 ROI was used for the other five animals. No difference in the sd between 3 mm^2 and 5 mm^2 was observed. The 3 mm^2 ROI visually appeared large enough to be representative of the TC site, but not so large as to include regions beyond that represented by a TC's value. For each animal, the pretreatment SI value, SI_0, for each TC site was the average of the values from the pretreatment images. Signal intensity values from images during and after treatment were graphed for comparison with SI_0.

Statistically, a change in SI was taken to be significant from SI_0 if it fell outside the range of $SI_0 \pm 2.58\ se_s$. The standard error, se_s, was calcu-

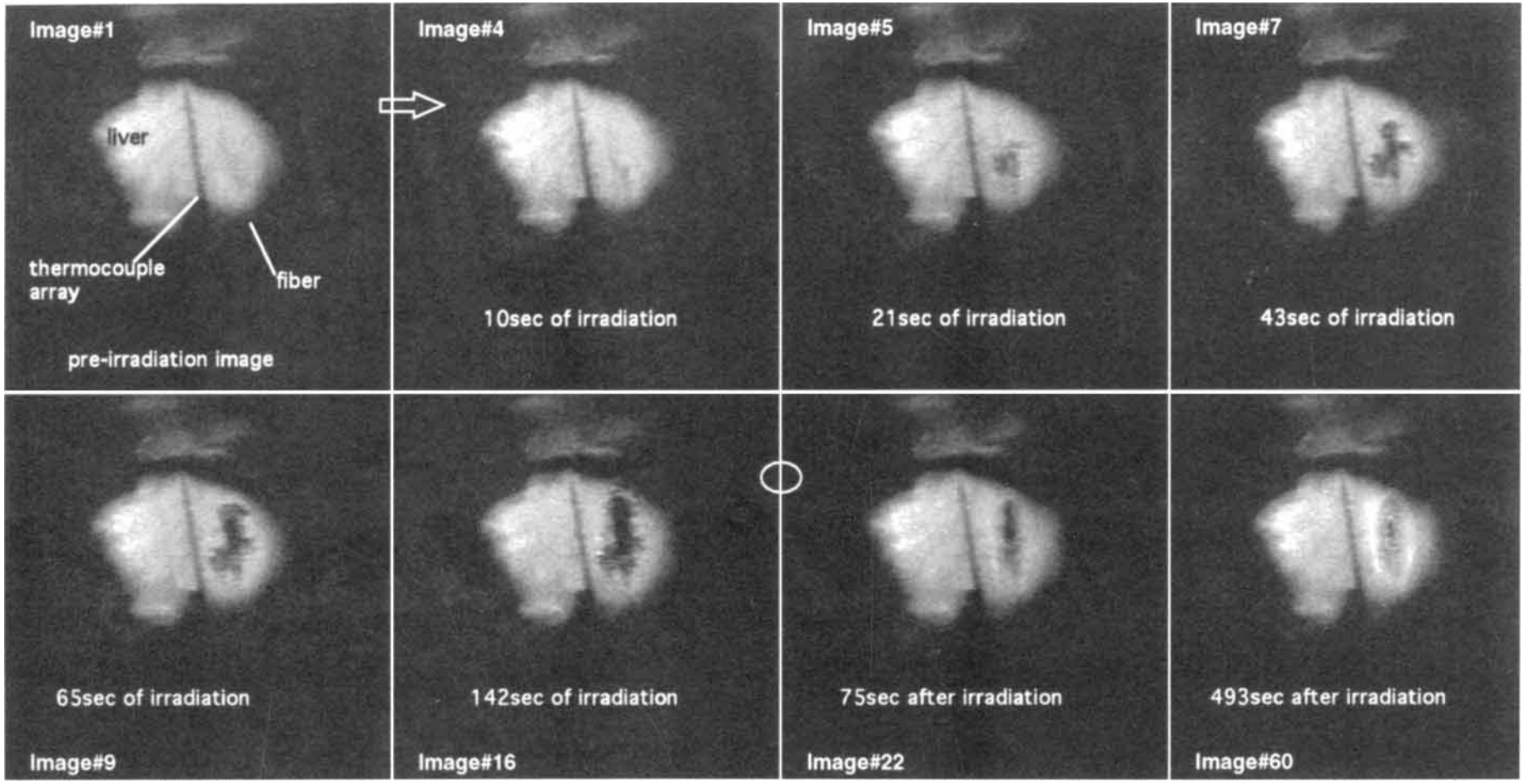

Fig. 2. Representative MRI from the 65 images acquired before, during, and after in vivo ILP in a rabbit liver at 1,064 nm with 3 W for 2.5 min. The T1-weighted fast spin-echo imaging technique used an 18 msec TE, 300 msec TR, 8 cm FOV, 256 × 128 resolution, and a slice thickness of 3 mm. Each took 10 sec to acquire. Annotation in the first image indicates the positions of the thermocouple array and the laser fiber. Each thermocouple is seen as a small shadow along the array on the side facing the fiber. As irradiation continued, a developing lesion was evident in the image plane. The reversible component dissipated after the laser had been turned off and the tissue cooled. Irreversible tissue changes persisted.

lated as $sd_0/\sqrt{N}$, where N is the number of pixels in the ROI. N = 225 for a 5 mm^2 ROI and 121 for a 3 mm^2 ROI [17].

Histology

After ILP was complete, the animal was removed from the magnet. On withdrawing the thermocouple array and the laser fiber, each was replaced in the liver by a thin segment of pasta, which served as a histologic marker. The lobe was excised and placed in formalin for 2 weeks. Each was then sectioned and stained with a hematoxylin and eosin stain. The two separate pieces of pasta remained in place and were used to identify a plane of tissue corresponding to that observed under MRI.

RESULTS

Imaging

Dynamic 10 sec acquisition of MR images at 1 second intervals showed the development of the ILP lesions in vivo (Fig. 2). Images acquired prior to laser irradiation showed a relatively uniform field of *hyper*intensity (bright, relative to the background) identifying the liver lobe in cross section. Some drop-off in SI radially across the image plane was inherent with the use of a surface imaging coil. The thermocouple array and laser fiber were identifiable as straight dark line segments.

During laser irradiation, a region of *hypo*intense SI (dark, relative to the background) developed around the tip of the fiber. Due to the short image acquisition time, the series of images shows the lesion's growth in the plane in ~2–3 mm increments along its length and width. This expansion slowed as the intraoperative lesions approached ~10 × 15 mm as seen under MRI. The intraoperative images exhibited asymmetries about the fiber axis, which varied from animal to animal, that is, hypointense lateral spikes and lobes extending outward.

After the laser was turned off, the hypointensity proved to be reversible. The reversal took place over the same time period as the cooling of the tissue. This revealed the underlying effect of the treatment seen as the permanent irreversible changes in the image (Fig. 3). In animal 4, MRI acquired 7.5 min post-irradiation showed a persistent hypointense region with a resemblance to the intrairradiation image. Around this final lesion was a concentric *hyper*intense (bright) margin. In contrast, MRI of animal 6 showed the hypointensity proved entirely reversible and the lesion was generally hyperintense with marked variability.

Histology was obtained for each of the animals. Stained tissue sections were ~15 μm thick. Several sections were cut for each fixed block of tissue. Each section contained a full or partial slice of the pasta markers, which identified the locations of the thermocouple array and laser fiber. A fully detailed correlation of the histology to the images is pending, but some specific examples are presented here (see Fig. 3).

In the data shown, post-laser MR images are placed side by side with histology. The full MR images have been cropped and magnified for the presentation and for comparison with the photos of the tissue sections. This magnification begins to show the pixels of which the image is composed (i.e., graininess). The examples illustrate correlations between the postoperative image and the histology. In both examples, the tissue shows a central vacuole, an adjacent outer affected zone, and an outer margin. In one case, however, the central vacuole was filled with blood serum and not in the other. This difference in tissue reponse is reflected in the MR images in which the empty vacuole is seen as permanently hypointense, whereas the fluid and tissue-filled example has a brightened center under MRI. Such results have been reportedly previously [10,13,14].

An outer affected zone surrounded the vacuoles and was composed of generally normal-looking hepatocytes, though scattered throughout were pockets and streams of severely thermally damaged red blood cells (RBCs). These were present within the sinuses between the hepatocytes. The RBCs were lacking in pigment and seemed reduced to membranes only. These "ghost" RBCs were evident with an oil immersion lens at 1,000× and have been reported as evidence of high temperatures in tissue. They have also been reported in a study of ILP in the brain [18]. This region of ghosts hepatocytes corresponds to the relative hyperintense region seen in the post-irradiation images. The actual mechanism of such a contribution to the MRI signal is still under discussion.

Beyond this region, there is an abrupt overabundance of normally pigmented RBCs filling the sinuses over an extended region. "Bulls-eye" type gradients of thermal ILP damage have been reported in the liver, including central cavitation and charring, surrounded by grades of coagulation with an abrupt distal change over into nor-

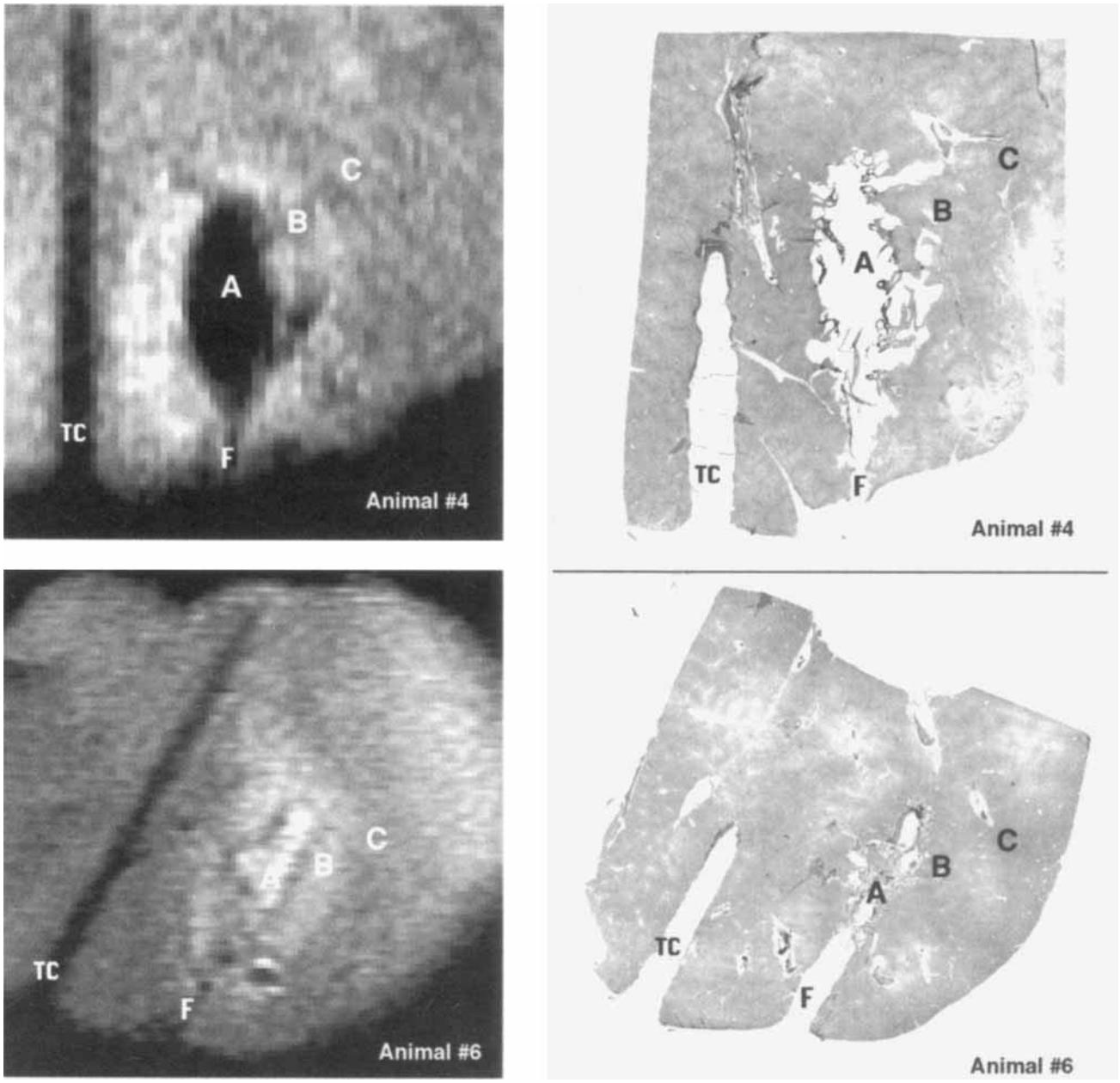

Fig. 3. **Top:** An MR image at ~7.5 min after laser irradiation stopped, and corresponding H & E stained histology section from tissue excised immediately after experiment for animal 4. **Bottom:** The same data for animal 6. The letters A, B, and C identify corresponding regions of the induced lesion. In animal 4, the central vacuole formed by the laser (A) is dark on MR and corresponds to a loss of tissue. In contrast, animal 6 shows a bright central area where tissue and serum are present. Both images show a relatively bright region (B), which corresponds to a region of relatively normal hepatocytes with intracellular spaces engorged with depigmented ghost RBCs as seen at 1,000× (not shown). Region C in the images contains seemingly normal hepatocytes and intracellular sinuses engorged with normal-looking RBCs.

mal tissue [1,10,13], similar to ILP in muscle, tumors, and brain [18–23].

Temperature Measurements

Eighteen temperature profiles were obtained—three for each of the six animals. The results from animal 1 are shown in Figure 4. In this example, the temperatures increased smoothly from starting values of 35°C by as much as +12.1°C at the proximal site and by +7.6°C at the distal site while the laser was on. The same data show a rate of temperature increase of

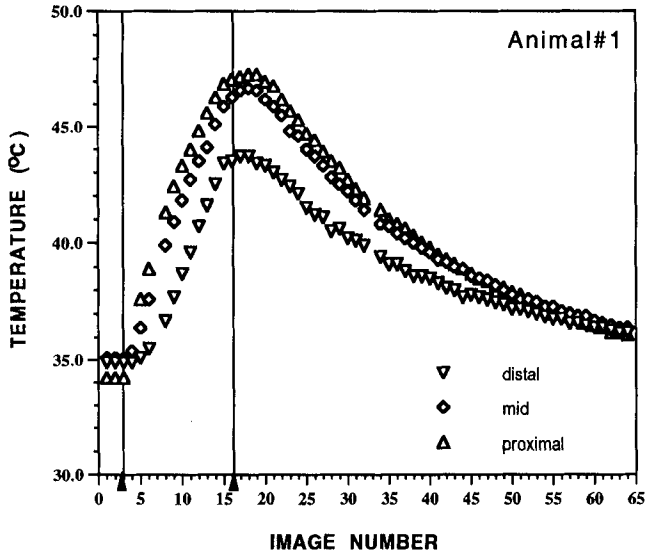

Fig. 4. Temperature measurements before, during, and after in vivo ILP in animal 1 at 1,064 nm with 3 W for 2.5 min. Measurements were made during the 1 sec interval between each 10 sec MR image acquisition. Arrowheads on the horizontal axis indicate the start of laser irradiation (at the end of image 3) and the finish (at the end of image 16).

~0.02°C/sec as calculated from the slopes of the linear portions of the curves. Notably, data from the other animals included temperature increases as high as +25.1°C and rates of change ranging from 0.02 to 0.16°C/sec.

Signal Intensity Measurements

Region of interest measurements taken at each of the thermocouple sites were plotted as a function of time (see Fig. 1). Thus, 18 graphs were generated from the three TC sites for the six animals. Overall, the values of SI behaved unpredictably, exhibiting instances of both increase and decrease from pretreatment values.

Figure 5 shows the three graphs for ILP in animal 4. At the site of the distal TC, the SI fluctuated randomly between hyper-intense and hypointense values; this was true during irradiation and carried on afterwards. At the site of the mid-TC, SI decreased significantly by 20% of the pretreatment value during irradiation. After the laser was turned off, the values increased gradually to values 20% greater than pretreatment values. At the proximal site, the intraoperative values appeared generally elevated throughout the entire irradiation and continued to increase postoperatively.

In summary, the SI values measured at the "distal" sites for all six animals indicated that intraoperatively three of the animals showed a mix of both unchanged and significantly *increased* values. By contrast, the other three showed a mix of both unchanged and significantly *decreased* values. Post-laser measurements showed values that were generally a mix of unchanged and *increased* values. In the "proximal" sites for all the animals, half the animals showed a general *increase* in SI during the laser irradiation; the values plateaued and maintained the same levels after the laser was turned off. In two cases (animals 4 and 5) the values increased substantially. The other half of the animals showed generally no change (animal 5) or a decrease (animals 2 and 6); postoperatively animal 5's values tended to increase, while those of animals 2 and 6 tended to return to baseline.

DISCUSSION

For our experiments, the T1-weighted FSE imaging sequence and the related MRI parameters were chosen for their speed and resolution: an 8 cm FOV and a 3 mm image slice thickness and with a 10 sec acquisition time for each image (with a 1 sec interval). Figure 2 demonstrates that MRI can follow the development of a laser induced lesion in vivo in liver. The time scale of the image acquisition presents a near real-time view of the thermal effects for laser parameters, which are relevant to human ILP applications [24–28].

Since the MRI signal had proven sensitivity to temperature and the nature of ILP is thermal, several previous studies emphasized this aspect. Such studies were done in parallel to the development of faster imaging techniques to deliver images on an appropriate time scale. Testing included ex vivo water-bath experiments to detail SI(T), and other experiments focused on MRI of ILP. A motivating hypothesis of temperature-sensitive MRI-guided ILP was that by "measuring" the temperature via SI values in real time, or sufficiently close to real time, the temperature could be mapped dynamically throughout the affected tissue volume. By following the temperature history of the tissue intraoperatively, the damage incurred could be predicted; accordingly, the light "dose" could then be adjusted and the surgery controlled.

In proving the hypothesis, it is crucial to confirm the relationship between SI and T for a particular imaging sequence and tissue type sub-

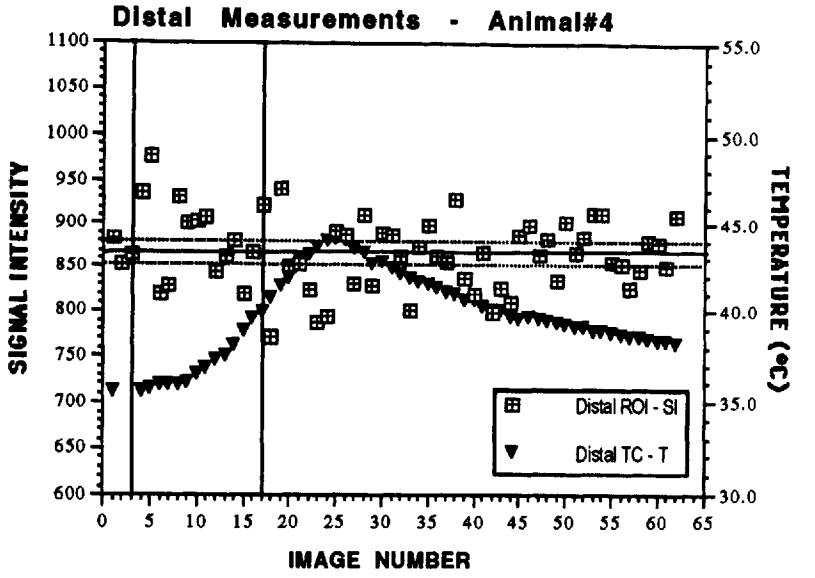

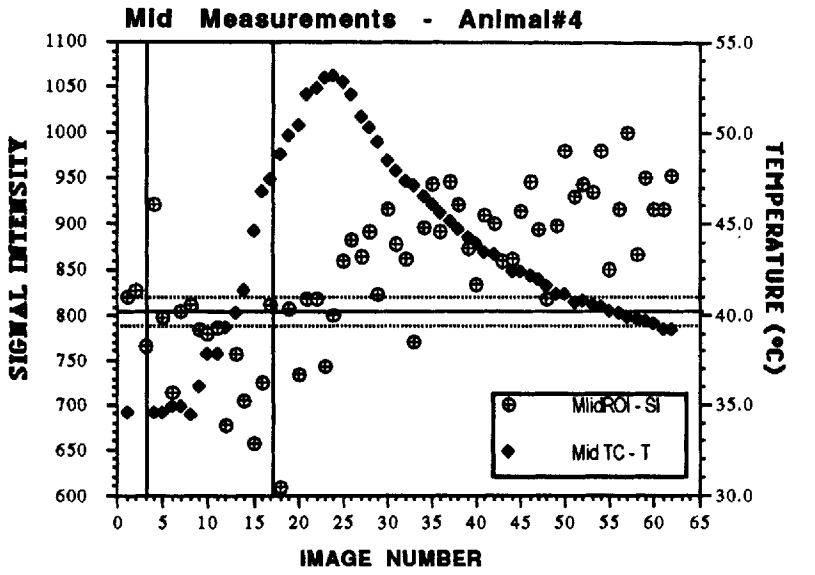

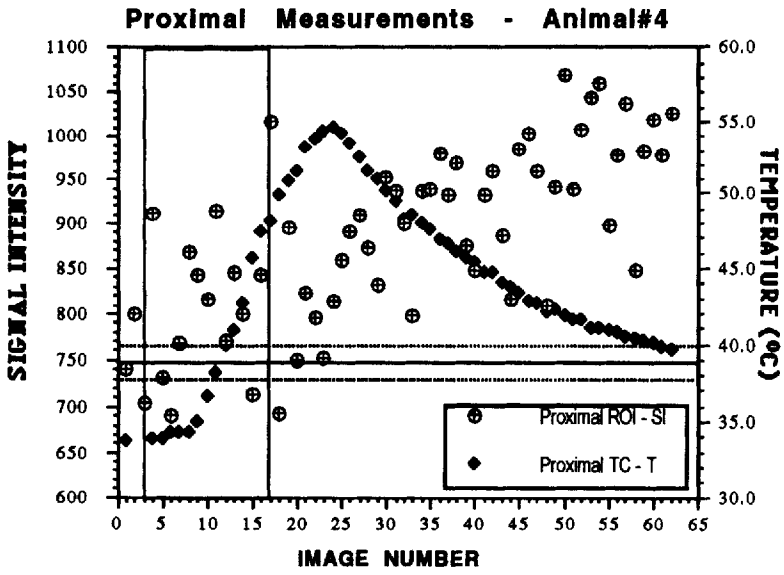

Fig. 5. Graphs of signal intensity (SI) during laser treatment are shown for all three thermocouple sites for animal 4. Vertical lines on the horizontal axis indicate the start and end of laser irradiation. The solid horizontal line marks the pretreatment SI value. The horizontal dashed lines indicate the region beyond which a change in SI is taken to be significant. Superimposed on each SI vs. image number graph is the corresponding temperature graphs using the right vertical axis.

jected in vivo to specified laser parameters. Fast, T1-weighted MRI has been shown to be among the most temperature sensitive, exhibiting a 0.5–1.1% decrease in SI per degree Celsius seen in ex vivo liver [14,15]. Previously reported ILP/temperature experiments were performed (1) with image acquisition times and spatial resolution as used in our experiments but with gels or inanimate tissue and not in vivo; (2) with the MRI temperature sensitivity tested over for $T < 60°C$ and not the full range of T encountered in ILP; and (3) to monitor ILP in vivo but with no detailed attention to temperature measurements or correlation with tissue damage [14–16]. Our experiments were implemented to fill in some of the necessary data to provide a detailed correlation between image, temperature, and tissue damage with the most clinically relevant application of the technologies involved.

In this first analysis, measured temperatures were compared to the SI values obtained as average values from ROIs positioned at the sites of the temperature measurements. As seen in Figure 5, the smooth increase of temperature by several degrees did not result in a commensurate smooth decrease in SI as expected. (A commensurate decrease in SI was expected from previous ex vivo calibrations of SI and T for this imaging sequence [14,15]. However, the irreversible thermally induced tissue effects of ILP can alter the tissue and change the baseline of the MR signal. Such hysteresis in SI vs. T curves for ex vivo tissue was seen in the earliest report on MRI of ILP [10].) In the examples, only the mid-TC showed a decrease of an appropriate magnitude during irradiation, tending toward a 20% decrease in SI for a 15°C increase as the laser was shut off. Notably, for this same site the SI increased to significantly elevated values as the tissue cooled, suggesting a contribution from a nonthermal mechanism to the MR signal. At the distal site in the example, SI fluctuated high and low in spite of a near 10°C increase. The proximal site showed a consistent increase in SI throughout treatment and afterwards.

That the SI values varied in our experiments as they did reflects the nature of the in vivo tissue irradiation and the manifestation of those effects as seen on MR. Although the temperatures were not high enough at the sites of measurement to induce a direct thermal effect on the tissue (dehydration, coagulation, or charring), a secondary effect at the periphery occurred related to the filling of the intrahepatic sinuses with normal and ghost RBCs. This effect opposed the reversible temperature induced SI changes. By documenting such effects, MR of ILP in various tissues will be understood and protocols for clinical application created.

A previous study on in vivo liver in rats used histology to study the progression of ILP lesions with time [1]. Combining that study's results with our own, it is likely that the hypointense region seen here with MRI may demarcate the region within which cellular degradation and necrosis occur postoperatively. Thus, while SI-dervived temperatures may not demarcate the damage zones for in vivo ILP liver treatments, the bright signal characteristic of a secondary thermal effect at the lesion edge may do so. Clinical application of MRI-ILP may then be achieved by characterizing the MRI "signature" of the ILP lesion in a given tissue for laser parameters. This signature will be understood in terms of the thermally induced direct and secondary effects, and incorporated into a surgical feedback-control system.

Thus, the lack of correlation between signal intensity values and temperature at the margins of the ILP lesions seen in this study do not refute the temperature sensitivity as exhibited in previous reports, nor does it disallow the usefulness of temperature-sensitive MRI for ILP. Rather, it addresses concerns about the translation of such findings into the in vivo experience. Although magnetic resonance imaging may not monitor temperature throughout the lesion well, it could be used to monitor the outermost periphery of the surgical site, or to monitor a leading edge of a temperature gradient moving toward nearby untargeted structures.

A detailed mapping of the histology of the MR images is necessary prior to further speculation on the actual mechanism involved; this mapping involves digitization of the stained sections, providing formats for comparison, and is pending from this laboratory. Such mapping will also provide information regarding the cause of the asymmetries seen in the images acquired during ILP. Further, data for a range of doses in a variety of tissues need to be collected so that MRI-guided ILP can be formulated into a widely accepted, minimally invasive surgical tool.

ACKNOWLEDGMENTS

The authors thank Randall Margolis, M.D., for his assistance to date in the assessment of the histology of the ILP treated tissue and Reiko Mat-

sumoto and Vincent Collucci for their assistance with the experiments. This work was sponsored by the Department of the Navy, Office of the Chief of Naval Research under the Medical Free Electron Laser Program (grant N00014-92-J-1597) and by NIH grant 5R01CA45743-05. The content of this report does not necessarily reflect the position of the government, and no official endorsement should be inferred. Certain technical support for this project was provided by Laserscope Surgical Systems, (San Jose, CA) and by GE Medical Systems (Milwaukee, WI).

REFERENCES

1. Mathewson K, Cooleridge-Smith P, O'Sullivan JP, Northfield TC, Bown SG. Biological effects of intrahepatic Nd:YAG laser photocoagulation in rats. Gastroenterology 1987; 93:550–557.
2. Wyman DR, Wilson B, Adams K. Dependence of laser photocoagulation on interstitial delivery parameters. Lasers Surg Med 1994; 14:59–64.
3. Masters A, Bown SG. Interstitial laser hyperthermia in the treatment of tumors. Lasers Med Sci 1990; 5:129–135.
4. Wyman Dr, Wilson BC, Malone DE. Medical imaging systems for feedback control of interstitial laser photocoagulation. Proc IEEE 1992; 80:890–902.
5. Jolesz FA, Blumenfeld SM. Interventional use of magnetic resonance imaging. Magn Reson Q 1994; 10:85–96.
6. Parker DL, Smith V, Sheldon P, Crooks LE, Fussel L. Temperature distribution measurements in two dimensional NMR imaging. Med Phys 1983; 10:321–325.
7. Bottomley PA, Foster TH, Argersinger RE, Pfeifer LM. A review of normal tissue hydrogen NMR relaxation times and relaxations mechanisms from 1–100MHz: Dependence on tissue type, NMR frequencey, temperature, species, excision and age. Med Phys 1984; 11:425–448.
8. Parker DL. Applications of NMR imaging in hyperthermia: an evaluation of the potential for localized tissue heating and non-invasive temperature monitoring. Proc IEEE 1984; 1:161–167.
9. Dickinson RJ, Hall AS, Hind AJ, Young IR. Measurement of changes in tissue temperature using MR imaging. J Comp Assist Tomogr 1986; 10:468–472.
10. Jolesz FA, Bleier AR, Jakab P, Ruenzel PW, Huttl K, Jako G. MR imaging of laser tissue interactions. Radiology 1988; 168:249–253.
11. LeBihan D, Delannoy J, Levin RL. Temperature mapping with MR imaging of molecular diffusion: Application to hyperthermia. Radiology 1989; 171:853–857.
12. Cline HE, Schenck JF, Walkins RD, Hyninen K, Jolesz FA. Magnetic resonance-guided thermal surgery. Magn Reson Med 1993; 30:98–106.
13. Higuchi N, Bleier AR, Jolesz FA, Colucci VM, Morris JH. Magnetic resonance imaging of the acute effects of interstitial Nd:YAG laser irradiation in tissue. Invest Radiol 1992; 27:814–821.
14. Matsumoto R, Oshio K, Jolesz. Monitoring of laser and freezing-induced ablation in the liver with T1-weighted MR imaging. J Magn Reson Imaging 1992; 2:555–562.
15. Matsumoto R, Mulkern RV, Hushek SG, Jolesz FA. Tissue temperature monitoring for thermal interventional therapy: Comparison of T1-weighted MR sequences. J Magn Reson Imaging 1994; 4:65–70.
16. Hushek SG, Morrison PR, Kernahan GE, Fried MP, Jolesz FA. Thermal contours from magnetic resonance images of laser irradiated gels. Proc Biomed Optics Eur 1993; 2082:52–59.
17. Bourke GJ, McGilvray. "Interpretation and Uses of Medical Statistics." Oxford: Blackwell Scientific, 1969:44–67.
18. Schober R, Bettag M, Sabel M, Ulrich F, Hessel S. Fine structure of zonal changes in experimental Nd:YAG laser-induced hyperthermia. Laser Surg Med 1993; 13: 234–241.
19. Mathewson K, Barr H, Tralan C, Bown SG. Low power interstitial Nd:YAG laser photocoagulation: Studies in a transplantable fibrosarcoma. Br J Surg 1989; 76:378–381.
20. Eggert HR, Kiessling M, Kleihues P. Time course and spatial distribution of neodymium yttrium aluminum garnet laser-induced lesions in the rat brain. Neurosurgery 1985; 16:443–448.
21. Tracz RA, Wyman DR, Little PB, Towner RA, Stewart WA, Schatz SW, Wilson BC, Pennock PW, Janzen EG. Comparison of magnetic resonance images and the histopathological findings of lesions induced by interstitial laser photocoagulation in the brain. Lasers Surg Med 1993; 13:45–54.
22. El-Quahabi A, Guttman CRG, Hushek SG, Bleier AR, Dashner K, Dikkes P, Black P, Jolesz FA. MRI guided interstitial laser therapy in a rat glioma model. Lasers Surg Med 1993; 13:503–510.
23. Dowlatshahi K, Babich D, Bangert JD, Kluiber R. Histologic evaluation of rat tumor necrosis by interstitial Nd:YAG laser hyperthermia. Lasers Surg Med 1992; 12: 159–164.
24. Bettag M, Ulrich F, Kahn T, Seitz R. Local interstitial hyperthermia in malignant brain tumors using low power Nd:YAG laser. Proc SPIE 1991; 1525:409–411.
25. Castro DJ, Lifkin RB, Saxton RE, Nyerges A, Soudant J, Layfield LJ, Jabour BA, Ward PH, Kangarloo H. Metastatic head and neck malignancy treated using MRI guided ILP: An initial case report. Laryngoscope 1992; 102:26–32.
26. Fan M, Ascher PW, Schrottner O, Ebner F, Germann RH, Kleinert R. Interstitial 1.06 Nd:YAG laser thermotherapy for brain tumors under real-time monitoring of MRI: Experimental study and phase I clinical trial. J Clin Laser Med Surg 1992; 10:355–361.
27. Dowlatshahi K, Bhattacharya AK, Silver B, Matalon T, Williams JW. Percutaneous interstitial laser therapy of a patient with recurrent hepatoma in a transplanted liver. Surgery 1992; 112:603–606.
28. Gewise B, Beuthan J, Fobbe F, Stiller D, Muller G, Boese-Landgraf J, Wolf K, Deimling M. MRI controlled laser-induced interstitial thermotherapy of the liver. Invest Radiol, 1994; 29:345–351.